ARTICLE

Co-nonsolvency in concentrated aqueous solutions of PNIPAM: effect of methanol on the collective and the chain dynamics

Received 00th January 20xx,
Accepted 00th January 20xx

DOI: 10.1039/x0xx00000x

Konstantinos N. Raftopoulos,*[a,†] Konstantinos Kyriakos,[a] Matthias Nuber,[a] Bart-Jan Niebuur,[a] Olaf Holderer,[b] Michael Ohl,[c] Oxana Ivanova,[b,§] Stefano Pasini,[b] and Christine M. Papadakis*[a]

The polymer dynamics in concentrated solutions of poly(*N*-isopropyl acrylamide) (PNIPAM) in D_2O/CD_3OD mixtures is investigated in the one-phase region. Two polymer concentrations (9 and 25 wt%) and CD_3OD contents in the solvent mixture of 0, 10 and 15 vol% are chosen. Temperature-resolved dynamic light scattering (DLS) reveals the collective dynamics. Two modes are observed, namely the fast relaxation of polymer segments within the blobs and the slow collective relaxation of the blobs. As the cloud point is approached, the correlation length related to the fast mode increases with CD_3OD content. It features critical scaling behavior, which is consistent with mean-field behavior for the 9 wt% PNIPAM solution in pure D_2O and with 3D Ising behavior for all other solutions. While the slow mode is not very strong in the 9 wt% PNIPAM solution in pure D_2O, it is significantly more prominent as CD_3OD is added and at all CD_3OD contents in the 25 wt% solution, which may be attributed to enhanced interaction between the polymers. Neutron spin-echo spectroscopy (NSE) reveals a decay in the intermediate structure factor which indicates a diffusive process. For the polymer concentration of 9 wt%, the diffusion coefficients from NSE are similar to the ones from the fast relaxation observed in DLS. In contrast, they are significantly lower for the solutions having a polymer concentration of 25 wt%, which is attributed to the influence of the dominant large-scale dynamic heterogeneities. To summarize, addition of cosolvent leads to enhanced large-scale heterogeneities, which are reflected in the dynamic behavior at small length scales.

Introduction

Stimuli-responsive polymers, in the form of aqueous solutions, microgels or hydrogels, attract significant attention due to their potential applications in e.g. drug delivery, sensing, or more recently, in artificial muscles.[1,2,3,4,5,6,7,8,9,10,11] These polymers undergo a conformational transition upon a change of an external stimulus in a very narrow range. The most widely studied stimulus is temperature, and the polymers responding to temperature changes are called thermoresponsive.

By far the most studied polymer of the kind is poly(*N*-isopropylacrylamide) (PNIPAM), which contains both hydrophilic and hydrophobic groups in its side groups and features lower critical solution temperature (LCST) behavior. For a large range of molar masses and polymer concentrations, its cloud point in water, T_{cp}, is ~32 °C. Below, PNIPAM is soluble in water, whereas above, it dehydrates to a certain extent, becomes insoluble and forms long-lived aggregates.[12,13,14,15,16,17,18] A recent review summarizes and discusses the findings on the phase behavior of PNIPAM in aqueous solution.[19]

At temperatures below T_{cp}, i.e. in the one-phase state of semidilute aqueous solutions of PNIPAM, concentration fluctuations were observed using small-angle neutron scattering.[20,21] The characteristic static correlation length follows scaling behavior with respect to temperature and polymer concentration. The scaling exponents were found to be slightly, but consistently lower than the ones predicted by mean-field theory, which was attributed to hydrogen bonding of PNIPAM with water.[20,21] While the concentration dependence of the correlation length points to water being a good solvent far below the spinodal temperature T_s, theta conditions are reached when approaching T_s.[22] A theoretical work points towards sequence formation of water molecules along the chain and cooperative dehydration at T_{cp} as the origin of the sharp transition.[16]

The dynamics of aqueous PNIPAM solutions were studied thoroughly in (very) dilute conditions with a focus on the hydrodynamic radius of the single chain.[13,22,23,24,25] Several studies address more concentrated solutions.[26,27,28,29,30,31,32] These use Raman spectroscopy to characterize the vibrational dynamics of the alkyl units,[31] dielectric relaxation spectroscopy to characterize the chain dynamics[28] as well as the rotational

[a] Technische Universität München, Physik-Department, Fachgebiet Physik weicher Materie, James-Franck-Str. 1, 85748 Garching, Germany
[b] Jülich Centre for Neutron Science at Lein Maier-Leibnitz Zentrum (MLZ), Forschungszentrum Jülich GmbH, Lichtenbergstr. 1, 85748 Garching, Germany
[c] Jülich Centre for Neutron Science JCNS-1, Forschungszentrum Jülich GmbH, Wilhelm-Johnen-Str., 52425 Jülich, Germany
† Present address: Konstantinos N. Raftopoulos, Cracow University of Technology, Department of Chemistry and Technology of Polymers, Warszawska 24, 31-155 Kraków, Poland
§ GSI Helmholtzzentrum für Schwerionenforschung GmbH, Planckstraße 1, 64291 Darmstadt, Germany

motions of PNIPAM monomer, and quasi-elastic neutron scattering (nENS) to investigate the water dynamics.[30,32] Dynamic light scattering (DLS) elucidates the collective dynamics, revealing two diffusive relaxation processes.[26,33] The fast process was attributed to the relaxation of chain segments between neighboring overlap points. The associated dynamic correlation length was in the range of a few nanometers and was attributed to the distance between overlap points of the chains or, equivalently, to the cooperative motion of chain segments within each blob. The corresponding diffusion coefficient was found to scale with concentration c as $c^{0.32\pm0.02}$ (ref. 26). The dynamic correlation lengths of the slow mode are of the order of a few 100 nm and were attributed to long-range concentration fluctuations.[26] Since this mode is only present in PNIPAM solutions in H_2O and in D_2O, but not in solutions in tetrahydrofurane, it was concluded that intermolecular interactions between PNIPAM chains through H_2O (or D_2O) bonds are at the origin of this mode.[26]

Addition of a cosolvent, e.g. a short-chain alcohol, alters the hydration behavior of the PNIPAM chain in aqueous solution.[34] This manifests itself in, among others, a strong dependence of the cloud point of PNIPAM on the solvent composition: Up to a certain volume fraction of cosolvent, T_{cp} is suppressed, then it increases sharply, which results in a miscibility gap at room temperature.[35,36,37] In dilute solution, the chain conformation in water/alcohol (methanol or ethanol) mixtures changes from expanded to collapsed, as cosolvent is added successively to the aqueous PNIPAM solution.[38,39,40] A quasi-elastic neutron scattering study on the solvent dynamics in a concentrated PNIPAM solution in an 85:15 v/v water:methanol mixture carried out by some of us revealed that, in the one-phase state, both solvents are attached to the chain.[41] The question arises in which way the chain dynamics and the collective dynamics are influenced by the presence of alcohol.

The vast majority of theoretical explanations of the co-nonsolvency effect is based on polymer-solvent interactions and the preferential adsorption of methanol to the PNIPAM chain compared to the one of water.[42,43,44,45,46,47] For instance, for PNIPAM dissolved in a mixture of water and methanol, the binding of both species with the chains is both cooperative and competitive: Although sequences of hydrated monomers and sequences of monomers solvated with methanol are formed, the repulsive interaction between hydrated monomers and monomers solvated by methanol results in chain contraction.[42,44] An alternative explanation is based on the formation of segmental loops due to bridging of the chain by methanol molecules, resulting in a compact chain conformation.[45] In another study, the preferential binding of methanol to PNIPAM was shown to lead to an increase in the configurational entropy of the globular state, inducing chain collapse.[46] Moreover, it was shown that, upon a slight increase in methanol content, the interaction energy between the polymer and the solvent molecules decreases strongly, thus driving the collapse of the chains.[46] Another investigation suggests that methanol mainly interacts with the hydrophobic isopropyl groups and water mainly with the hydrophilic amide groups and that the competition between the two types of solvent molecules leads to geometric frustration and the collapse of the chains.[47] In a recent investigation, solvent-mediated interactions are proposed to be of key importance.[48] We note that all of these theoretical approaches are concerned with the static chain conformations. We are not aware of any predictions regarding the changes of the dynamics, for instance the single chain dynamics or the collective dynamics, of aqueous solutions of thermoresponsive polymers upon addition of a cosolvent. However, the above predictions concerning the changes of chain conformation may lead to substantial alterations of the dynamics.

Here, we investigate the dynamics solutions of PNIPAM solutions in water/methanol mixtures having rather low methanol contents (0-15 vol%). We choose polymer concentrations of 9 and 25 wt%), which are in the concentrated regime. However, in both cases, the chains are fully hydrated, and bulk solvent is present. We characterize the collective concentration fluctuations by DLS and the chain dynamics by neutron spin-echo (NSE) spectroscopy. The aim of our study is to reveal the role of the cosolvent on the dynamics in line with the theoretical predictions described above.

?CDerimental

Materials

PNIPAM (molar mass 36.0 kg mol^{-1}, dispersity 1.26) was purchased from Sigma Aldrich, Munich, Germany. Heavy water (D_2O, purity 99.90%) and fully deuterated methanol (CD_3OD, purity 99,80%) were purchased from Deutero GmbH, Kastellaun, Germany. All components were used as received. Stock mixtures of D_2O/CD_3OD at CD_3OD volume fractions of 0, 10 and 15 vol% were prepared, and PNIPAM was dissolved in these solvent mixtures at mass fractions of 9 and 25 wt%. The solutions were agitated on a laboratory shaker in sealed vials, until the polymer was fully dissolved. In order to prevent clouding, especially in the solutions with high CD_3OD content, ice packs were also placed on the shaker and changed regularly.

The overlap concentration c^* is estimated from the weight-average molar mass of the polymer, M_w, and its radius of gyration, T_g, by $c^* \approx 3M_w/(4\pi N_A T_g^3)$.[49] Using $M_w \approx 45$ kg mol^{-1} and the value of $T_g \approx 18$ nm determined by some of us previously for the same polymer in dilute aqueous solution at 20 °C,[50] c^* is found at 0.32 wt%. In an 80:20 v/v mixture of water and methanol, the radius of gyration of PNIPAM was found to be ca. 18 % lower than in pure water,[38] i.e., the gyration volume is lower by a factor of ~0.5. The PNIPAM concentrations of 9 and 25 wt% are safely above c^*.

Cloud Doint determination

The cloud points were determined experimentally as follows. A few ml of the solution was placed in a glass vial in a

temperature-controlled toluene bath. The temperature was increased in steps of 0.5 °C. At each temperature, the sample was equilibrated for 1 min, before it was briefly removed and inspected. The first temperature where the solution was found to be cloudy was considered as the cloud point.

Fynamic liGht scatterinGHFLI J

For DLS, an instrument comprising an ALp-5000/E correlator (ALp-Laser pertriebsgesellschaft mbH, Langen, Germany), an ALp/SO-SIPD photomultiplier to which the signal was fed by an optical fiber and a HeNe laser operated at 35 mW (wave length λ o 632.8 nm) and a goniometer was used. The sample was mounted in an index-matching vat, which was filled with toluene and thermostated by a JULABO F32 thermostat (JULABO Labortechnik GmbH, Seelbach, Germany).

The viscous solutions were mounted in cylindrical cuvettes. Temperature-dependent measurements were performed starting at low temperature and heating towards the respective cloud points, in steps of 2 °C, at a detection angle of 90°. After each temperature change, the samples were allowed to equilibrate for 5 min. Intensity autocorrelation functions $F_2(\tau)$ were measured in 3 consecutive runs of 10 min duration. Angle-dependent measurements were performed from 30 to 150° in steps of 10°. The momentum transfers Uwere calculated as Uo $4\pi n \times \sin(\theta/2)/\lambda$. The refractive index of the solutions, *n*, were measured independently with an Abbe refractometer at 20 °C, resulting in *n* o 1.3445 and 1.3833 for the 9 and 25 wt % solutions in D_2O and *n* o 1.3455 and 1.3646 for the solutions in 80:20 v/v D_2O/CD_3OD, respectively. The values for solutions with intermediate solvent compositions (10 and 15% CD_3OD) were calculated by linear interpolation and were used for all temperatures.

The autocorrelation functions were analyzed by fitting the sum of one single and one stretched exponential function to the $F_2(\tau)$ data:

$$\boldsymbol{G_2}!\boldsymbol{\tau}" -\mathbf{1} \# \boldsymbol{C} \$\boldsymbol{A_{fast}}\mathbf{exp}!-\frac{\boldsymbol{\tau}}{\boldsymbol{\tau_{fast}}}" \% \boldsymbol{A_{slow}}\mathbf{exp}!-!\frac{\boldsymbol{\tau}}{\boldsymbol{\tau_{slow}}}^{\boldsymbol{\beta_{slow}}} \&^2 \quad (1)$$

where H is the intercept, V_{fast} and V_{slow} are the relative amplitudes of the fast and the slow decay, V_{fast} q V_{slow} o 1, τ_{fast} and τ_{slow} the relaxation times and β_{slow} the stretching exponent of the slow mode. The fraction of the slow mode is given by V_{slow}. After fitting, the normalized intensity autocorrelation functions $g_2(\tau)$ -1 o r$F_2(\tau)$ -1s/H were calculated using the H-values determined in the fit. For the 9 wt% solution in pure D_2O, the slow mode is rather broad, and the average relaxation time

$$\langle \boldsymbol{\tau_{slow}} \rangle \# \boldsymbol{\tau_{slow}} \frac{r!^{\mathbf{1}/\boldsymbol{\beta_{slow}}}"}{\boldsymbol{\beta_{slow}}} \quad (2)$$

was used for further evaluation, where Γ(W/ denotes the Gamma function. In all other solutions, β_{slow} was close to unity, and τ_{slow} was used directly.

The dynamic correlation length corresponding to the fast mode, ξ_{fast}, was calculated by

$$\boldsymbol{\xi_{fast}} \# \frac{\boldsymbol{k_B T}}{\boldsymbol{6\pi\eta D_{fast}}} \quad (3)$$

where k_B is Boltzmannts constant and *T* the absolute temperature. η is the dynamic viscosity of the solvent. For D_2O, the temperature-dependent values of H_2O from ref. 51 were used. For the solvent mixtures, data from ref. 52 were inter- and extrapolated using the pogel-Fulcher-Tammann relation. D_{fast} denotes the diffusion coefficient, which is calculated by

$$\boldsymbol{D_{fast}} \# !\boldsymbol{\tau_{fast}}\boldsymbol{q}^{\mathbf{2}"-\mathbf{1}} \quad (4)$$

Neutron sDin echo sDectroscoDy HNI ?J

NSE experiments were performed using the instruments J-NSE of the Jülich Centre for Neutron Science outstation at the Heinz Maier-Leibnitz uentrum (MLu), Garching, Germany,[53,54,55] and SNS-NSE at the Spallation Source at Oak Ridge National Laboratory, U.S.A.[56,57]

At J-NSE,[53,54,55] the measured Fourier times ranged from 0.1 ns to 60 ns and were extended to 100 ns for the lowest U-values (0.03 and 0.05 v^{-1}). Each measurement in a range of momentum transfers Uo 0.03-0.21 v^{-1} (corresponding to a range of length scales of ca. 3-21 nm) took ca. 24 h. The samples were mounted in Hellma nuartz cells of size 30 mm × 30 mm with a sample thickness of 2 mm for 9 wt% solutions and 1 mm for 25 wt%. The sample temperature was controlled by circulating thermostated water through the sample holder. Experiments were performed at 24 °C (except in one case, where the temperature was 25 °C) and at few additional temperatures between 22 and 31 °C. Grafoil or graphite powder were used to measure the resolution function of the spectrometer. The detector was a multiwire area detector. The instrument parameters are described elsewhere.[55]

At SNS-NSE,[56,57] the 25 wt% solution in pure D_2O was measured at 27.5 and 30.5 °C and the 25 wt% solution in D_2O/CD_3OD at 22.0, 25.0 and 27.0 °C at U-values in the range 0.03-0.21 v^{-1}. The samples were mounted in 2 mm quartz cells. The final U-values are a result of grouping/integrating over certain wavelengths bands and scattering angles. The wavelengths were chosen between 9-12 v resulting in a Fourier time range between 40 ps and 50 ns. The sample temperature was controlled with pressurized air in the so called temperature forcing system (TFS). The measurement time for the whole Useries at a single temperature was approx. 30 h. Grafoil was used to measure the resolution function. The detector was a multiwire area detector.

The NSE data were fitted with a stretched exponential function:

$$\frac{S(q,t)}{S(q,0)} = \exp\left(-(\Gamma_{NSE}t)^{\beta_{NSE}}\right) \quad (5)$$

Γ_{NSE} is the relaxation rate, and β_{NSE} the stretching exponent. The average relaxation rate $\langle\Gamma_{NSE}\rangle$ was calculated from

$$\langle\Gamma_{NSE}\rangle = \frac{\beta_{NSE}}{\Gamma(1/\beta_{NSE})}\Gamma_{NSE} \quad (6)$$

The diffusion coefficient D_{NSE} was determined by

$$D_{NSE} = \langle\Gamma_{NSE}\rangle q^2 \quad (7)$$

Results and discussion

In this section, we first report the cloud points. Then, the DLS and NSE results elucidating the collective and the chain dynamics at temperatures below the cloud point are presented and compiled.

Cloud Doints

The measured cloud points of the solutions having PNIPAM concentrations of 9 wt% and 25 wt% are given in dependence on the volume fraction of CD_3OD in Table 1. As expected, they decrease with increasing CD_3OD content for both concentrations.[34,35,36,37] The value obtained for the PNIPAM solutions in pure D_2O, 33 °C, is consistent with the one previously reported for the same polymer at the intermediate PNIPAM concentration of 13 wt% in D_2O, namely 32.9 °C.[21]

TaLle MN Cloud points T_{cp} and critical temperatures T_c in dependence on PNIPAM concentration and CD_3OD content

PNIPAM concentration HDtPJ	**CF$_E$QF volume fraction** HPJ	**Cloud Doint** T_{cp} HRCJ	**Critical temDerature** T_c HRCJ
9	0	33.0± 0.5	35.1 ± 0.1[(a)] 35.1 ± 0.2[(b)]
	10	29 ± 0.5	32.8 ± 0.3[(b)]
	15	27 ± 0.5	28.6 ± 0.4[(b)]
25	0	33 ± 0.5	34.1 ± 0.6[(b)]
	10	29 ± 0.5	29.4 ± 0.2[(b)]
	15	27 ± 0.5	26.7 ± 0.3[(b)]

(a) from the fit with v o 0.50, (b) from the fits with v o 0.63

DLS measurements were carried out between (in most cases) 12 °C and T_{cp}, i.e. in the one-phase state. Angle-dependent measurements reveal the nature of the two dynamic processes identified. For NSE measurements, all samples were measured at 24 °C (except the 25 wt% solution in 90:10 vol/vol D_2O/CD_3OD, which was measured at 25 °C) in dependence on momentum transfer. Moreover, measurements were carried out at temperatures ~2 °C and ~5 °C below the respective cloud points, i.e. in the one-phase state.

Collective concentration fluctuations

The temperature dependence of the collective concentration fluctuations in all solutions was studied by DLS in pure D_2O and in 90:10 and 85:15 vol/vol D_2O/CD_3OD. For both polymer concentrations and all solvent compositions, the normalized autocorrelation functions $g_2(\tau)$ -1 feature two decays (Figure 1): A fast relaxation appears in the time range of ~0.001-1 ms for both polymer concentrations and a slow relaxation above ~10 ms for the 9 wt% solutions and above ~100 ms for the 25 wt% solutions. For the 9 wt% solutions, addition of CD_3OD results in a strong increase of the relative amplitude of the slow mode, which may be attributed to stronger correlations between the large-scale dynamic heterogeneities. For the 25 wt% solutions, the relative amplitude of the slow mode is very high at all CD_3OD contents, and the decay is only partially visible in the accessible time window. For all samples, the relative amplitude of the slow mode decreases with increasing temperature, when the cloud point is approached.

ARTICLE

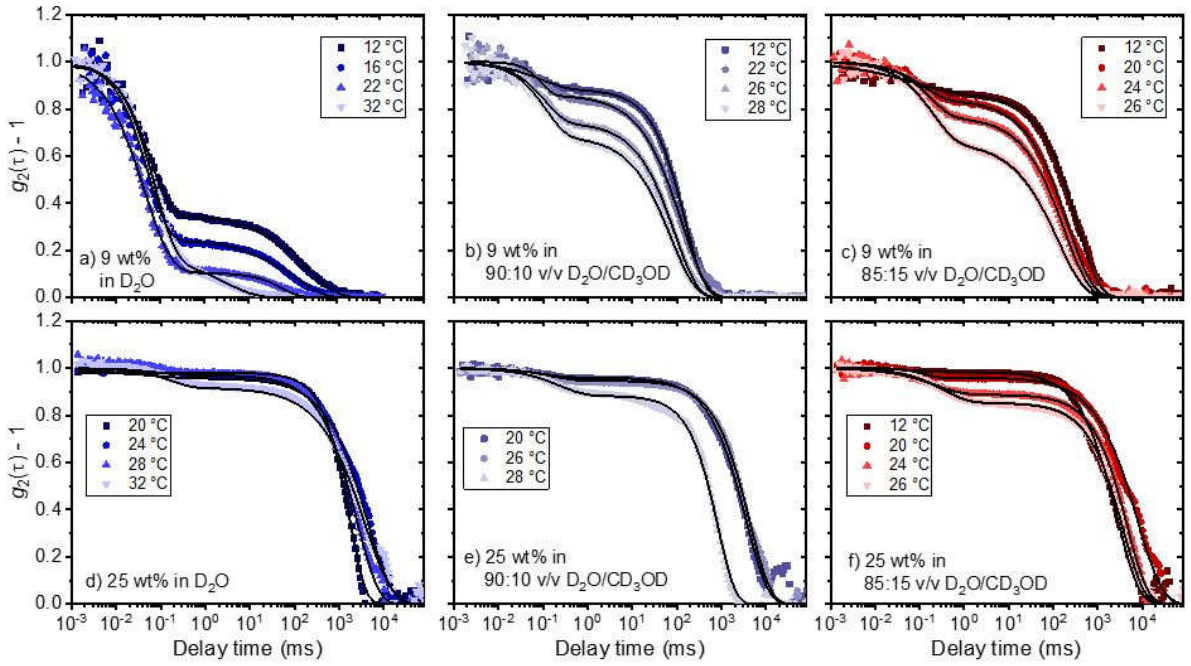

Figure 1. Representative normalized intensity autocorrelation functions from DLS, $g_2(\tau)$ - 1, for polymer concentrations of (a-c) 9 wt% and (d-f) 25 wt% at the temperatures and solvent compositions given in the graphs. The lines are fits of eq. 1.

The fact that two modes are present with the slow mode being dominant indicates that the solutions are above the overlap concentration,[26,58] see the Experimental Section. Previously, the fast process was attributed to the relaxation of chain segments between neighboring overlap points[33] or, in other words, to the cooperative motion of monomers within a blob, and its relaxation rate Γ_{fast} was found to be proportional to q^2.[26,58,59] The second, broad decay at longer correlation times (above ~10 ms) was previously assigned to long-range dynamic heterogeneities[26] or to the relaxation of a cage, which is formed by a number of correlated blobs[60] thus, it is related to interchain interactions. Its relaxation rate was previously found to depend on the momentum transfer like $\Gamma \propto q^x$ with 2 x α x 3.[26] In semidilute, aqueous PNIPAM solutions, it was attributed to long-range, correlated concentration fluctuations, associated with hydrogen bonding of PNIPAM with water or with the strong interaction between the PNIPAM chains in a poor solvent.[58] Both explanations involve dynamics at length scales larger than the size of the single chain, i.e. collective phenomena resulting in large-scale dynamic heterogeneities.

To characterize the relaxation times, the widths of the decays as well as the relative amplitudes of the two decays, the sum of two stretched exponentials was fitted to the autocorrelation functions (eq. 1, Figure 1). We first discuss the slow mode. Its fraction, measured at a scattering angle of 90°, is shown in dependence on temperature in Figure 2a and d. For a polymer concentration of 9 wt% in pure D_2O, it decreases from ~0.6 at 12 °C to ~0.4 at temperatures of 20 °C and above (Figure 2a), and it is relatively broad ($\beta_{slow} \cong$ 0.37-0.86, Figure 2b). For 10 and 15 % of CD_3OD, the relative amplitude of the slow mode at 12 °C is 0.93, i.e. significantly higher than in pure D_2O, and it decreases to 0.82-0.84 for both solvent mixtures, as the cloud point is approached (Figure 2a). At these CD_3OD contents, the slow decay is steeper ($\beta_{slow} \cong$ 0.67-1.06, Figure 2b). Figure 2c shows that, upon heating, the relaxation times τ_{slow} decrease from ~1 to 0.02 s for the solution in pure D_2O (for this solution, we consider $\langle\tau_{slow}\rangle$, calculated using eq. 2), from 0.3 to 0.2 s for 10 % CD_3OD and from 0.7 to 0.3 s for 15 % CD_3OD.

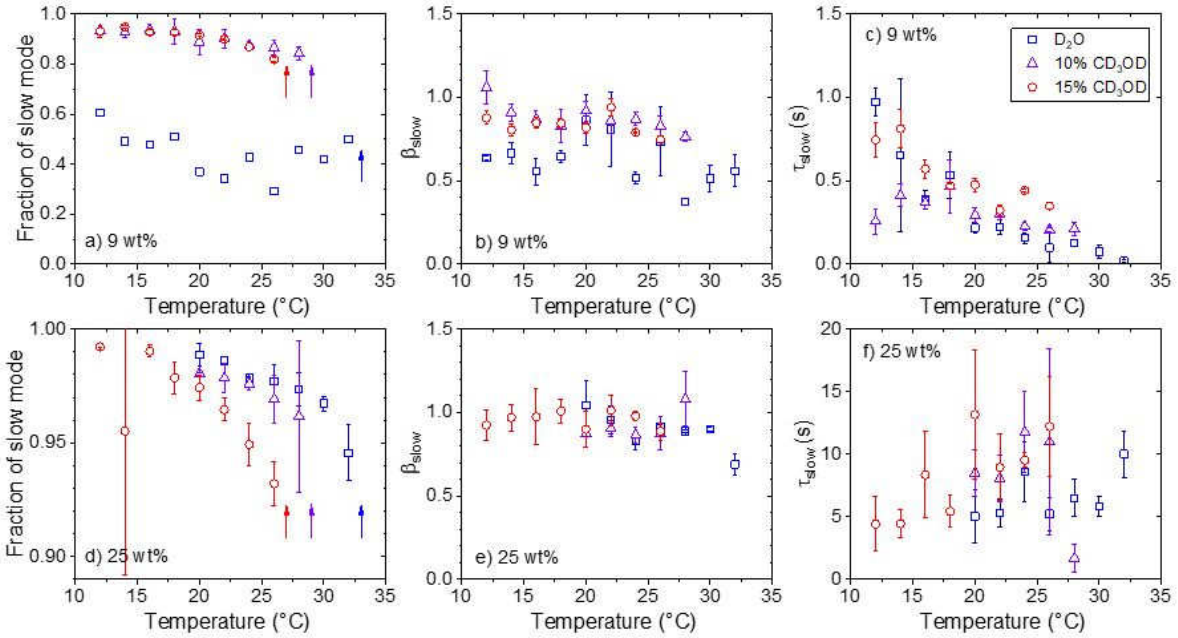

SIGure AN Characteristics of the slow mode in the DLS autocorrelation functions for PNIPAM concentrations of (a-c) 9 wt%, (d-e) 25 wt%. (a, d) Fraction of the slow mode at a scattering angle of 90 °, (b, e) stretching exponent β_{slow} and (c, f) relaxation time τ_{slow} in dependence on temperature at the CD_3OD contents given in (c) For the sample with 9 wt% in pure D_2O, $\langle\tau_{slow}\rangle$ is shown, calculated using eq. 2. The arrows in (a, b) indicate the cloud points T_{cp}.

At 25 wt%, the slow mode dominates strongly at all solvent compositions and at all temperatures (Figure 2d-f). For all solvent compositions, its relative amplitude decreases with temperature, starting at ~0.98-0.99 at the lowest temperature and decreasing to values of ~0.93-0.96 just below the cloud point, and seems to decrease slightly with increasing CD_3OD content (Figure 2d). The opposite behavior of the relative amplitude of the slow mode with CD_3OD content in the 9 and the 25 wt% solution may reflect counteracting effects of polymer-polymer interactions and polymer-solvent interactions. However, it may also be due to the fact that, for the 25 wt% solutions, the relaxation times of the slow mode are very high (in the range of ~2-13 s, Figure 2f), and therefore, the decay is partially outside the accessible time range. The decays seem closer to single-exponential than at 9 wt% (Figure 2e), but again, this seems to be a consequence of the high relaxation times.

To identify the nature of the decays, angle-dependent DLS experiments were performed. The relaxation rates of the fast and the slow mode in dependence on the square of the momentum transfer, U², are shown in Figure 3. At both polymer concentrations, the inverse relaxation times of the fast mode are proportional to U² (Figure 3a, c), and the fast mode can be assigned to the cooperative motion of monomers within a blob.58,59

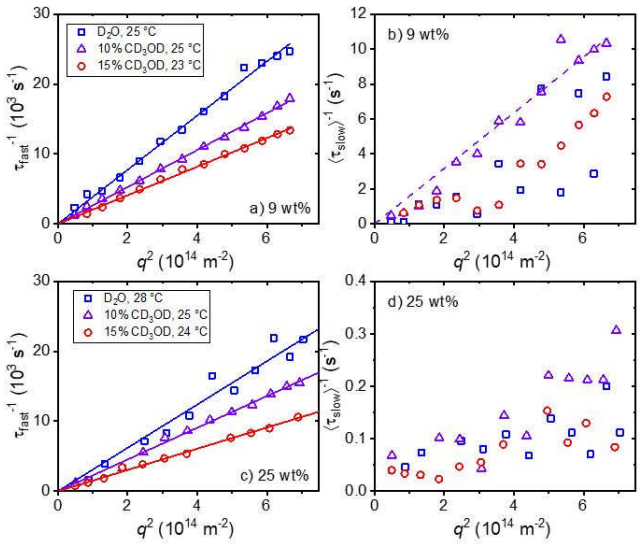

SIGure EN U dependence of the inverse relaxation times from DLS for polymer concentrations of (a, b) 9 wt% and (c, d) 25 wt%. The solvent compositions and the temperatures are given in the graphs. (a, c) Symbols: τ_{fast}. The lines are linear fits through the origin. (b, d) Symbols: $\langle\tau_{slow}\rangle$. The dashed line in (b) is a linear fit through the data from the solution in 90:10 v/v D_2O/CD_3OD.

In contrast to the fast mode, the inverse average relaxation time of the slow mode is not proportional to U², but the values are rather scattered. Only at a polymer concentration of 9 wt% in 90:10 vol/vol D_2O/CD_3OD, a linear behavior is approximately observed (Figure 3b), and a tentative determination of the diffusion coefficient using eq. 4 results along with eq. 3 in a correlation length of ~12 ym, which is outside the range of DLS.

The diffusion coefficients of the fast mode, D_{fast}, are calculated from the τ_{fast} values determined in the temperature scans at θ o 90° using eq. 4 (Figure 4). To eliminate effects of the proximity to the cloud point, we plot them in dependence on T z T_{cp}. All reported diffusion coefficients are higher than the ones reported for PNIPAM in aqueous solution in the semidilute regime.[26] At both polymer concentrations, the values decrease with increasing temperature, and the values from the solutions with 0 and 10 % CD_3OD are virtually equal, while the ones from the solutions with 15 % CD_3OD are distinctly lower. For given temperatures, the D_{fast} values of the 25 wt% solutions are slightly smaller than the ones of the 9 wt% solutions, which is not consistent with the scaling relation $D_{fast} \propto c^{0.32\pm0.02}$ reported for the same concentration range for aqueous solutions of PNIPAM.[26] We attribute the different concentration behavior to the strong large-scale dynamic heterogeneities in the solutions, which present domains with different dynamics, and D_{fast} is a value that is averaged over these domains.

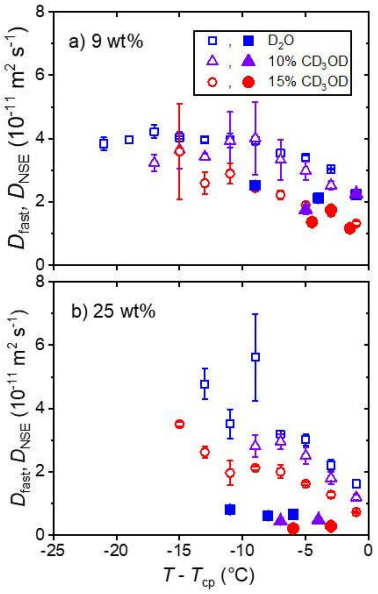

SIGure KNTemperature-dependent diffusion coefficients in dependence on T z T_{cp} for polymer concentrations of (a) 9 wt% and (b) 25 wt%. The solvent compositions are given in (a). Open symbols: values from the fast mode in DLS, closed symbols: values from NSE.

The dynamic correlation lengths of the fast mode, ξ_{fast}, are calculated from the diffusion coefficients D_{fast} using eq 3 along with the temperature-dependent viscosity of the solvent mixture (Figure 5). For both polymer concentrations, ξ_{fast} range between ~3 and ~25 nm, i.e. below and above the estimated radius of gyration (~18 nm, see the Experimental Section).

ξ_{fast} increases with temperature and with CD_3OD content. The temperature behavior can be described by the following model characteristic of critical scaling:

$$\xi_{fast} \# \xi_0 ! ! T_c - T " / T_c " ^{-\nu} \quad (8)$$

where ν is the critical exponent and T_c the critical temperature.

Fitting eq. 8 to the data from the 9 wt% solution in pure D_2O results in an exponent ν o 0.50 ± 0.01 and a critical temperature T_c o 35.1 ± 0.2 °C and provides a good fit to the data. T_c is higher than the cloud point (31 ± 1 °C), as expected. The value of the exponent ν resulting from this fit is equal to the one predicted by mean-field theory for the static correlation length (ν o 0.5). For all other datasets, leaving all three fitting parameters free results in large uncertainties. Therefore, we fix the exponent at ν o 0.50, which results in good fits for both polymer concentrations and all CD_3OD contents (dashed lines in Figure 5a,c). The resulting critical temperatures are added to Table 1.

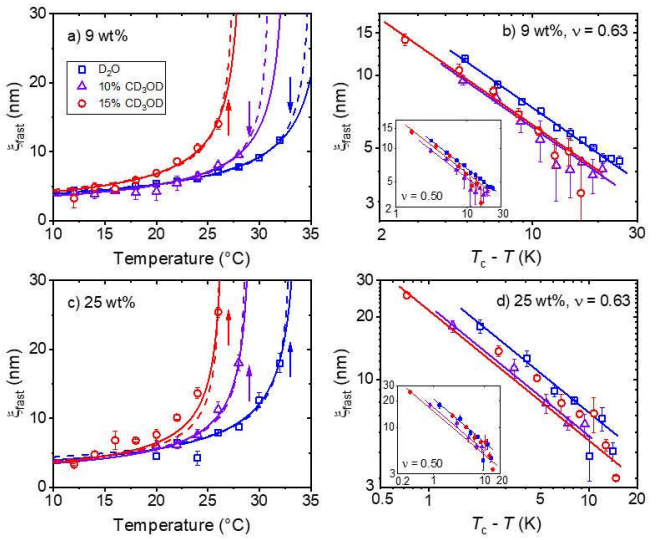

SIGure VN(a) Temperature dependent dynamic correlation length ξ_{fast} from DLS for the fast mode of all solutions at a polymer concentration of 9 wt% (a, b) and 25 wt% (c, d) and the CD_3OD contents given in (a). The dashed and full lines in (a) and (c) are fits of eq. 8 with ν fixed at values of 0.50 or 0.63, respectively. The arrows mark the cloud points T_{cp}. (b, d) Same data as in (a, c), plotted in a double-logarithmic representation of vs. T_c-T including the fitting curves, using the values of the fitting parameters obtained for ν o 0.63. The insets in (b) and (d) show the same data along with fits of eq. 8 with the exponent ν being fixed at 0.50.

As an alternative, we use the value of ν o 0.63, which was predicted for 3D Ising behavior and was previously observed in polymer solutions close to the critical temperature.[61,62,63] For the 9 wt% and 25 wt% solutions in pure D_2O, these fits are indistinguishable from the ones in which ν was fixed at 0.5 in the range explored experimentally. Judging from the reduced χ values, the fits with ν o 0.63 are slightly better than the ones with ν o 0.50 for all solutions (9 and 25 wt%) except the one with the polymer concentration of 9 wt% in pure D_2O. Possibly, this tendency towards 3D Ising behavior is related to the large-scale dynamic heterogeneities, which are very prominent in the cases where ν o 0.63 provides the better fits.

A parameter emerging from the fits of eq. 8 to the ξ_{fast} data is the critical temperature T_c. The values are given in Table 1. They decrease with increasing polymer concentration and with increasing content of CD_3OD and are slightly higher than the cloud points T_{cp}. The behavior of the dynamic correlation lengths is in agreement with the one of the static correlation

lengths reported for PNIPAM in D_2O of similar polymer concentrations: For polymer volume fractions of 0.0783 and 0.213, the exponent ν increases from 0.451 to 0.569.[20] The values of the static correlation lengths reported in this study at 23 °C are ca 1.67 and 1.04 nm, respectively. Thus, the ratios of the dynamic and the static correlation lengths are $\xi_d/\xi_s \approx 4$ and 6 for the low and high concentration, respectively. These values are of the same order of magnitude, but higher than the values around 2, which were reported for semidilute solutions of polystyrene (M_w o 10^5 g mol^{-1}, concentration 0.1 g mL^{-1}) in organic solvents.[64]

In Figure 5b and d, the ξ_{fast} data along with the fits with ν o 0.63 are replotted in log-log representation as a function of T_c z T, and the linear behavior confirms the validity of eq. 8. Since the same ν value describes the data from both polymer concentrations and all CD_3OD contents, the dynamic behavior of the motion of the monomers within the blobs seems to be unaffected by the cosolvent. (For comparison, the fits with ν o 0.50 are shown in the insets.) The graphs show that, for both polymer concentrations, ξ_{fast} decreases upon addition of CD_3OD for the same T_c z T values and that the values are very similar for 10 and 15 % of CD_3OD. Thus, the dynamics of the motion within the blobs is affected by the presence of CD_3OD, but is similar for 10 and 15% CD_3OD.

Thus, using DLS, two relaxation modes are identified in the one-phase regime, which were known from PNIPAM in pure D_2O, namely a fast one, attributed to the cooperative motion of segments within the blobs, and a slow one, attributed to long-range dynamic heterogeneities or, in other words, to the relaxation of a cage, which is formed by a number of correlated blobs. In the 9 wt% solution, the slow mode is particularly pronounced at CD_3OD contents of 10 and 15%, and it is very prominent at all CD_3OD contents for a polymer concentration of 25 wt%. For all solutions having a polymer concentration of 9 wt%, the slow decay is fully in the accessible time window of DLS. It is broad in pure D_2O, but close to single-exponential at the higher CD_3OD contents. In contrast, at 25 wt%, it is not fully within the accessible time window and the large-scale heterogeneities cannot be fully characterized. For all solutions studied, the fast mode shows the expected diffusive behavior $\Gamma_{fast} \propto U^2$, and the associated related dynamic correlation length follows $\xi_{fast} \propto |T$ z $T_c|^{-\nu}$. For the solution with a polymer concentration of 9 wt%, ν o 0.5, i.e. the mean-field prediction, fits the data best, whereas for all other solutions, 3D Ising behavior (ν o 0.63) gives slightly better agreement with the data. The critical temperatures T_c are slightly higher than the respective cloud points T_{cp}.

Chain dynamics

NSE experiments were performed to study the chain dynamics.[65,66] The U-values chosen for NSE (0.03-0.21 v^{-1}) cover the range over which the static concentration fluctuations typically decay.[67] We note that the length scales corresponding to these U-values are in the range of the Kuhn length of PNIPAM (40 v).[68]. Because these U-values are significantly larger than the ones probed in DLS (x 3×10^{-3} v^{-1}), we expect to observe the chain dynamics at smaller length scales. The samples were measured at temperatures 21-32 °C, always below the respective cloud point, i.e. in the one-phase state.

Figures 6 and 7 show the resulting representative normalized intermediate scattering functions @U,t)/@U,0) at polymer concentrations of 9 and 25 wt%, respectively. They show a single decay, which is attributed to density fluctuations on molecular length scales. For the solutions with the higher polymer concentration, the decays are significantly slower than at the lower polymer concentration, as expected. The @U,t)/@U,X) curves could be fitted with a stretched exponential function (eq. 5), giving the relaxation rate Γ_{NSE} and the stretching exponent, β_{NSE}. According to initial fits, the value β_{NSE} o 0.63 describes the data best, being indicative of main chain dynamics. This value was fixed throughout to obtain accurate values for Γ_{NSE}. The deviation from a single exponential decay may in part be ascribed to the polydispersity of the polymer, but also to the nature of the dynamic process. Due to the scatter of the data and the (in some cases) limited time range, other values of β also give satisfactory fits, and we refrain from using this parameter to identify a specific dynamic process.[69,70] Overall, the fits obtained in this way are good. Only for the 25 wt% solution with 15 % CD_3OD, slight deviations are present (Figure 6f and g).

ARTICLE

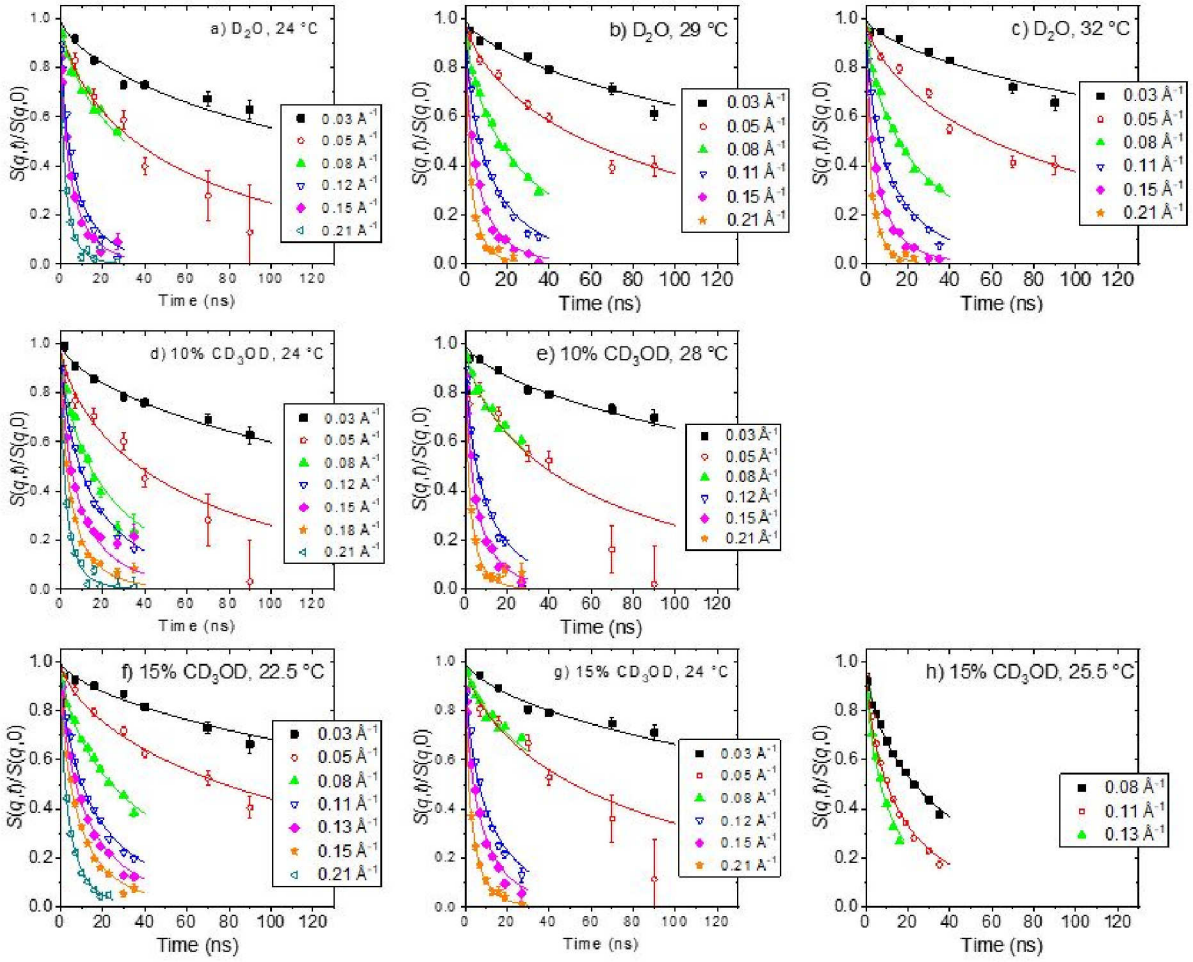

Figure 6. Representative intermediate scattering functions $S(q,t)/S(q,0)$ from NSE on the solutions having a polymer concentration of 9 wt% in pure D_2O (a-c) or containing 10 % (d,e) or 15 % CD_3OD (f-h) at the temperatures and q values given in the graphs. Lines are fits of stretched exponentials as described in the text.

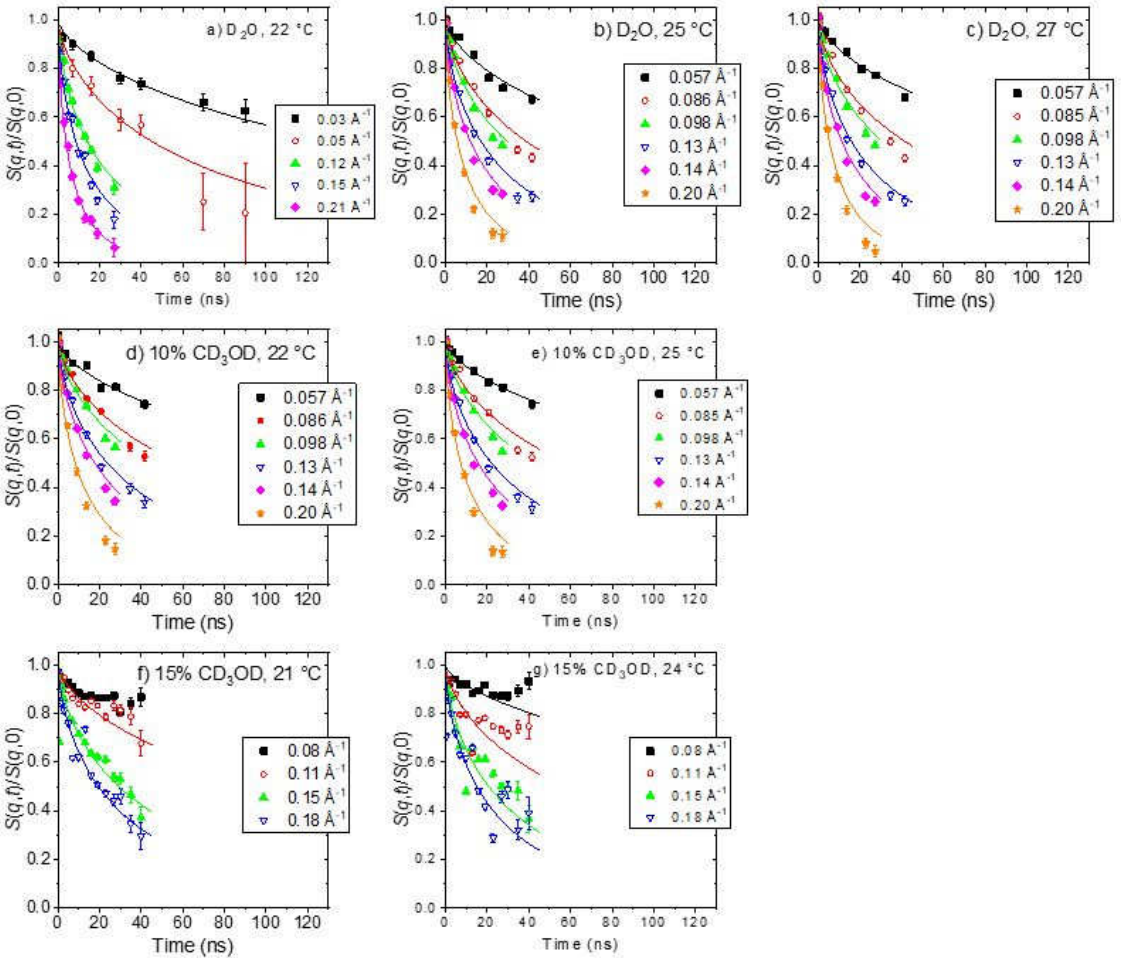

SIGure UNRepresentative intermediate scattering functions @U,t)/@U,0) from NSE on the solutions having polymer concentrations of 25 wt% in pure D_2O (a-c) or containing 10 % (d,e) or 15 % CD_3OD (f,g) at the temperatures and Uvalues given in the graphs. Lines are fits of stretched exponentials as described in the text.

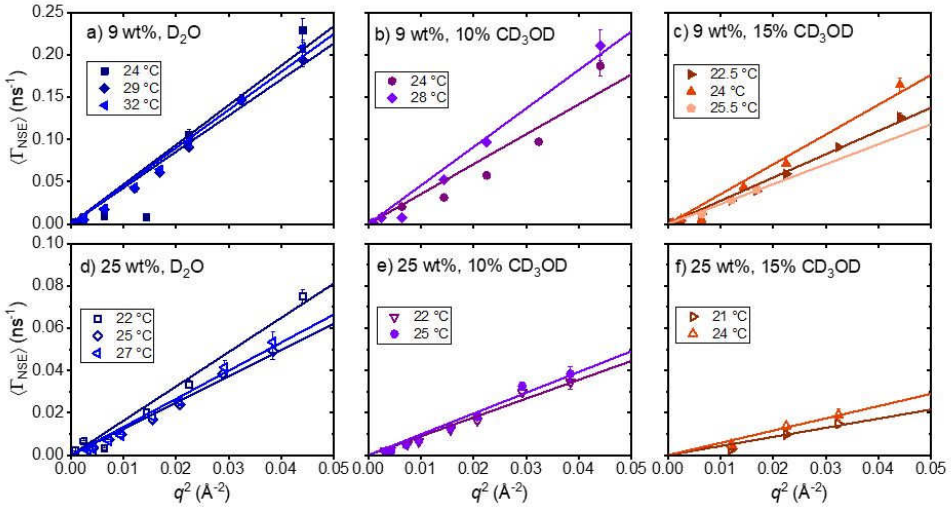

SIGure VWRelaxation rates $\langle\Gamma_{NSE}\rangle$ vs U² resulting from model-fitting the intermediate structure factors from NSE measurements on the solutions having polymer concentrations of 9 wt% (a-c) and 25 wt% (d-f) in pure D_2O (a, d) or containing 10 % CD_3OD (b, e) or 15 % CD_3OD (c, f) at the temperatures given in the graphs. Symbols: experimental data, full lines: linear fits in the same colors as the respective data.

ARTICLE

The resulting average relaxation rates $\langle\Gamma_{NSE}\rangle$ (eq. 6) are plotted vs. Q^2 to determine the nature of the dynamics (Figure 8). For diffusional dynamics, $\langle\Gamma_{NSE}\rangle$ is expected to be proportional to Q^2, which is indeed observed at all temperatures and for all solvent mixtures. The diffusion coefficients, as determined from the slopes of the linear fits of $\langle\Gamma_{NSE}\rangle$ vs. Q^2 are compared with the ones from the fast mode in DLS (Figure 4). While for the polymer concentration of 9 wt%, the agreement between DLS and NSE is excellent, deviations are observed in the values for 25 wt%. For instance, the values from NSE at 24-25 °C are a factor of ~4.4-7.0 lower than the ones from DLS at the same temperature. The reason for this discrepancy may be the enhanced large-scale dynamic heterogeneities in the latter solutions. The diffusion coefficients obtained by NSE are averaged over both types of dynamic domains. Due to the significantly larger Q-values, i.e. the smaller length scales probed in NSE, the diffusion coefficient may appear reduced compared to the fast mode probed in DLS.

Conclusions

The dynamics of two concentrated solutions of PNIPAM in D_2O/CD_3OD is investigated in dependence on the solvent composition in the one-phase state with the aim of characterizing the effect of co-nonsolvency on the collective and the chain dynamics. Theory predicts changes of the hydration layer of the PNIPAM chains upon addition of a cosolvent, resulting in a chain contraction. Based on that, we expected that these conformational changes have a strong effect on the chain dynamics as well as on the dynamics of the polymer segments within a blob. Since the polymer-polymer interactions may be altered by the addition of cosolvent as well, we address rather high polymer concentrations.

DLS reveals two relaxation modes. The fast mode is attributed to the relaxations of chain segments within the blobs. The corresponding correlation length increases with CD_3OD content, as the cloud point is approached, which is consistent with the expected chain contraction. Its scaling behavior with temperature is consistent with the expression from mean-field theory for the 9 wt% solution in pure D_2O, whereas all other solutions are slightly better described by the scaling law for 3D Ising behavior. We suspect that the latter behavior observed at small length scales is related to the particularly strong large-scale dynamic heterogeneities obvious from the dominant slow mode in these solutions. This dominance may be attributed to an enhanced interaction between the polymers mediated by the cosolvent in the solutions far above the overlap concentration.

While DLS probes the collective dynamics, NSE monitors the dynamics on the chain level and at smaller length scales, allowing to explore details of the diffusive motion. A single decay is observed, which can be described by a stretched exponential function, and which is diffusive. The resulting diffusion coefficients coincide with the ones from the fast relaxation observed in DLS at the lower polymer concentration. For the more concentrated solution, the values from NSE are a factor of ~4.4-7.0 lower, and we attribute this discrepancy to the dynamic heterogeneities at large length scales. In the NSE experiment, the diffusion coefficient is an average over these two types of dynamic domains, which leads to a shift towards lower values.

We conclude that, with the methods used, shifts of the relaxation times and the corresponding diffusion coefficients and correlation lengths are observed upon addition of up to 15 vol% of CD_3OD, but no qualitative changes. A correspondence between the fast segmental dynamics and the large-scale heterogeneities is found. We note that the present systems z concentrated polymer solutions in aqueous solution with a cosolvent z realize a more complex situation than the one described by current theories for co-nonsolvency, which seem to address the static behavior of single chains exclusively. More experimental and theoretical work is needed to bridge this gap.

Conflicts of interest

There are no conflicts to declare.

AcXnoOledGements

K.N.R. acknowledges a generous fellowship (TUFF) by the TUM University Foundation. We thank Deutsche Forschungsgemeinschaft (PA 771/14-1) for funding. We gratefully acknowledge Deutscher Akademischer Austauschdienst for the travel support within the program {Hochschulpartnerschaften mit Griechenland|. We thank K.-L. Claude, C.-H. Ko, P. Wastian (all TU München), E. Giannakopoulou and A. Kyritsis (both National Technical University of Athens, Greece) for help with the experiments and fruitful discussions. A portion of this research is based on experiments performed at the NSE instruments operated by JCNS at the Heinz Maier-Leibnitz uentrum (MLu), Garching, Germany, and at the Spallation Neutron Source, a DOE Office of Science User Facility operated by the Oak Ridge National Laboratory, U.S. A. We thank these facilities for allocating beamtime and providing excellent equipment.

Notes and references

1 (1) R. Pelton, VYv. HJGBiY Zterlace @i., 2000, WW, 1.
2 (2) M. A. Cohen Stuart, W. T. S. Huck, J. Genzer, M. Müller, C. Ober, M. Stamm, G. B. Sukhorukov, I. Szleifer, p. Tsukruk, M. Urban, F. Winnik, S. uauscher, I. Luzinov and S. Minko, *NatKre Mater.,* 2010YZ, 101.
3 (3) M. A. Ward and T. K. Georgiou, *PJGymers P[aseG*, 2011, E, 1215.
4 (4) A. S. Hoffman, VYv. DrKg. DeGv. Tev., 2013, TV, 10.
5 (5) E. G. Kelley, J. N. L. Albert, M. O. Sullivan and T. H. Epps III, Hhem. @c. Tev., 2013, KA, 7057.
6 (6) M. Hruby, S. K. Filippov and P. Štěpánek, \Kr. PJGym. J., 2015, TV, 82.
7 (7) J.-P. Couturier, M. Sütterlin, A. Laschewsky, C. Hettrich and E. Wischerhoff, Vngew. Hhem. Zt. \Y., 2015YVK, 6641.
8 (8) H. R. Culver, J. R. Clegg and N. A. Peppas, Vcc. Hhem. Tes., 2017YVB, 170.
9 (9) A. Nojoomi, H. Arslan, K. Lee and K. }um, *Nat.* HJmmKn., 2018, Z, 3705.
10 (10) P. Sanchez-Moreno, J. de picente, S. Nardecchia, J. A. Marchal and H. Boulaiz, *NanJmateriaG*, 2018, W, 935.
11 (11) W. H. Tao and u. G. He, Vsian J. Pharm. @i., 2018, ME, 101.
12 (12) H. G. Schild, PrJg. PJGym. @i., 1992, MU, 163.
13 (13) C. Wu and S. uhou, MacrJmJGcKGes, 1995, AW, 8381.
14 (14) A. p. Gorelov, A. Du Chesne and K. A. Dawson, *Physica* V, 1997, AKB, 443.
15 (15) ~. Wang, ~. niu and C. Wu, MacrJmJGcKGes, 1998, EM, 2972.
16 (16) }. Okada and F. Tanaka, MacrJmJGcKGes, 2005, EW, 4465.
17 (17) p. Aseyev, S. Hietala, A. Laukkanen, M. Nuopponen, O. Confortini, F. E. Du Prez and H. Tenhu, *PJGymer,* 2005, KT, 7118.
18 (18) F. Tanaka, T. Koga, I. Kaneda and F. M. Winnik, *J. Phys.*] HJnYens. Matter, 2011, AE, 284105.
19 (19) A. Halperin, M. Kr ger and F. M. Winnik, Vngew. Hhemie Zt. \Y., 2015, VK, 15342.
20 (20) M. Shibayama, T. Tanaka and C. C. Han, *J.* Hhem. Phys., 1992, ZU, 6829.
21 (21) A. Meier-Koll, p. Pipich, P. Busch, C. M. Papadakis and P. Müller-Buschbaum, NangmKir, 2012, AW, 8791.
22 (22) K. Kubota, S. Fujishige and I. Ando, *PJGym. J.,* 1990, AA, 15.
23 (23) C. Wu and ~. Wang, *Phys.* Tev. Nett., 1998, WB, 4092.
24 (24) ~. Wang and C. Wu, MacrJmJGcKGes, 1999, EA, 4299.
25 (25) R. Kita and S. Wiegand, MacrJmJGcKGes, 2005, EW, 4554.
26 (26) G. }uan, ~. Wang, C. C. Han and C. Wu, MacrJmJGcKGes, 2006, EZ, 3642.
27 (27) }. Ono and T. Shikata, *J.* Vm. Hhem. @c., 2006, MAW, 10030.
28 (28) S. Nakano, }. Sato, R. Kita, N. Shinyashiki, S. }agihara, S. Sudo and M. }oneyama, *J. Phys.* Hhem. [, 2012, MMT, 775.
29 (29) M. Füllbrandt, R. von Klitzing and A. Sch nhals, @lt *Matter,* 2012, W, 12116.
30 (30) M. Philipp, K. Kyriakos, L. Silvi, W. Lohstroh, W. Petry, J. J. Krüger, C. M. Papadakis and P. Müller-Buschbaum, *J. Phys.* Hhem. [, 2014, MMW, 4253.
31 (31) B.-J. Niebuur, K.-L. Claude, S. Pinzek, C. Cariker, K. N. Raftopoulos, p. Pipich, M.-S. Appavou, A. Schulte and C. M. Papadakis, VH@MacrJ Nett., 2017, T, 1180.
32 (32) B.-J. Niebuur, W. Lohstroh, M.-S. Appavou, A. Schulte and C. M. Papadakis, MacrJmJGcKGes, 2019, VA, 1942.
33 (33) T. L. }u, W.-C. Lu, W.-H. Liu, H.-L. Lin and C.-H. Chiu, *PJGymer,* 2004, KV, 5579.
34 (34) C. Scherzinger, A. Schwarz, A. Bardow, K. Leonhard and W. Richtering, HKrr. ^ p. HJGBiY Zterl. @i., 2014, MZ, 84.
35 (35) F. M. Winnik, H. Ringsdorf and J. penzmer, MacrJmJGcKGes, 1990, AE, 2415.
36 (36) H. G. Schild, M. Muthukumar and D. A. Tirrell, MacrJmJGcKGes, 1991, AK, 948.
37 (37) R. O. R. Costa and R. F. S. Freitas, *PJGymer,* 2002, EA, 5879.
38 (38) G. uhang and C. Wu, *J.* Vm. Hhem. @c., 2001, MAE, 1376.
39 (39) C. K. Chee, B. J. Hunt, S. Rimmer, I. Soutar and L. Swanson, @lt *Matter,* 2011, U, 1176.
40 (40) F. Wang, }. Shi, S. Luo, }. Chen and J. uhao, MacrJmJGcKGes, 2012, KV, 9196.
41 (41) K. Kyriakos, M. Philipp, L. Silvi, W. Lohstroh, W. Petry, P. Müller-Buschbaum and C. M. Papadakis, *J. Phys.* Hhem. [, 2016, MAB, 4679.
42 (42) F. Tanaka, T. Koga and F. M. Winnik, *Phys.* Tev. Nett., 2008, MBM, 028302.
43 (43) J. Pang, H. }ang, J. Ma and R. Cheng, *J. Phys.* Hhem. [, 2010, MMK, 8652.
44 (44) F. Tanaka, T. Koga, H. Kojima, N. ~ue and F.-M. Winnik, MacrJmJGcKGes, 2011, KK, 2978.
45 (45) D. Mukherji, C. M. Marques and K. Kremer, *NatKre* HJmmKn., 2014, V, 4882.
46 (46) F. Rodr guez-Ropero, T. Hajari and N. F. A. van der pegt, *J. Phys.* Hhem. [, 2015, MMZ, 15780.
47 (47) A. Pica and G. Graziano, *Phys.* Hhem. Hhem. Phys., 2016, MW, 25601.
48
(48) S. Bharadwaj and N. F. van der pegt, MacrJmJGcKGes, 2019, VA, 4131.
49 (49) H. Fujita, *PJGymer @IKtiJns,* Elsevier, Amsterdam, 1990.
50 (50) B.-J. Niebuur, L. Chiappisi, ~. uhang, F. Jung, A. Schulte and C. M. Papadakis, VH@MacrJ Nett., 2018, U, 1155.
51 (51) piscosity of Waterzpiscosity Table and piscosity Chart. https://wiki.anton-paar.com/en/water/ (accessed November 2018).
52 (52) S. u. Mikhail and W. R. Kimel, *J.* Hhem. \ng. Data, 1961, T, 533.
53 (53) M. Monkenbusch, R. Sch tzler and D. Richter, *NKcG ZstrKm. Meth*JYs *Phys.* Tes., 1997, EZZ, 301.
54 (54) O. Holderer, M. Monkenbusch, R. Sch tzler, H. Kleines, W. Westerhausen and D. Richter, *Meas. @i. Techn*JG, 2008, MZ, 034022.
55 (55) Heinz Maier-Leibnitz uentrum et al., *J. Grge-scaG research IaciGies* 2015, M, A11.
56 (56) M. Ohl, M. Monkenbusch, D. Richter, C. Pappas, K. Lieutenant, T. Krist, G. usigmond and F. Mezei, *Phys.* [HJnY. *Matt.,* 2004, EVB, 147.

57 ([57]) M. Ohl, M. Monkenbusch, N. Arend, T. Kozielewski, G. pehres, C. Tiemann, M. Butzek, H. Soltner, U. Giesen, R. Achten, H. Stelzer, B. Lindenau, A. Budwig, H. Kleines, M. Drochner, P. Kaemmerling, M. Wagener, R. M ller, E. B. Iverson, M. Sharp and D. Richter, *NKcG ZstrKm. Meth*JYs *Phys. Tes.,* 2012, TZT, 85.

58 [58] G. }uan, ~. Wang, C. C. Han and C. Wu, *Macr*J*m*JGcKGs, 2006, EZ, 6207N

59 ([59]) S. Kunugi, K. Kameyama, T. Tada, N. Tanaka, M. Shibayama and M. Akashi, [*ra*MGan *J. Me*Y. [*i*JGTes., 2005, EW, 1233.

60 ([60]) J. Wang and C. Wu, *Macr*J*m*JGcKGs, 2016, KZ, 3184.

61 ([61]) R. Kita, K. Kubota and T. Dobashi, *Phys. Tev.* \, 1998, VW, 793.

62 ([62]) J. Jacob, M. A. Anisimov, J. p. Sengers, p. Dechabo, I. K. }udin and R. W. Gammon, V*pp*G^ *pt.,* 2001, KB, 4160.

63 ([63]) }. B. Melnichenko, G. D. Wignall and W. A. van Hook, \KrJ*phys.* N*ett.,* 1999, KW, 372.

64 ([64]) W. Brown and K. Mortensen, *Macr*J*m*JGcKGs, 1988, AM, 420.

65 ([65]) J. Colmenero and A. Arbe, *J. P*JG*ym. @i., Part* [ ] *P*JG*ym. Phys.,* 2013, VM, 87.

66 ([66]) I. Hoffmann, HJGiY *P*JG*ym. @i.,* 2014, AZA, 2053.

67 ([67]) K. Kyriakos, M. Philipp, J. Adelsberger, S. Jaksch, A. p. Berezkin, D. M. Lugo, W. Richtering, I. Grillo, A. Miasnikova, A. Laschewsky, P. Müller-Buschbaum and C. M. Papadakis, *Macr*J*m*JGcKGs, 2014, KU, 6867.

68 ([68]) C. G. Lopez, A. Scotti, M. Brugnoni and W. Richtering, *Macr*J*m*JGH*hem. Phys.*, 2019, AAB, 1800421.

69 ([69]) C. Scherzinger, P. Lindner, M. Keerl and W. Richtering, *Macr*J*m*JGcKGs, 2010, KE, 6829.

70 ([70]) D. Richter, M. Monkenbusch, A. Arbe and J. Colmenero, *NeKtrJn @in \ch*J *in P*JG*ymer @ystems*, Springer, Berlin Heidelberg, 2005.